doi:10.3788/gzxb20184701.0124002

基于半环结构的法诺共振透射特性研究

郭媛,许雪梅,尹林子,丁一鹏,董莉荣
(中南大学 物理与电子学院,长沙 410083)

摘 要:基于表面等离子激元理论提出一个由金属-介质-金属波导和半环切口组成的波导结构,应用时域有限差分法研究了该结构的透射特性.仿真结果表明:透射光谱中产生一个类似法诺共振线形的共振谷,该法诺共振由半环切口中连续态与离散态的相互干涉所致,其共振波长可以通过改变半环切口的结构参量进行调节,该结构灵敏度约为 575 nm/RIU,品质因数可达 5 671.添加一个矩形谐振腔于该结构上可产生多重法诺共振,品质因数为 6 555,此特征能为波导结构的设计提供极大的灵活性,有望在光学集成回路、纳米传感器方面得到比较广泛的应用.

关键词:表面等离子激元;纳米传感器;时域有限差分法;法诺共振;半环切口;波导结构
中图分类号:O436 **文献标识码**:A **文章编号**:1004-4213(2018)01-0124002-8

Study on the Transmission Characteristics of the Fano Resonance Based on the Semi-ring Structure

GUO Yuan, XU Xue-mei, YIN Lin-zi, DING Yi-peng, DONG Li-rong
(*School of Physics and Electronics, Central South University, Changsha* 410083, *China*)

Abstract: Based on the theory of Surface plasmon polaritons, a plasmonic structure consisting of a metal-insulator-metal waveguide and a semi-ring stub was proposed to investigate the transmission properties by the finite-difference time-domain method. Simulation results show that there is a sharp and asymmetric Fano profile in transmission spectrum, which originates from the interference between a discrete state and a continuous state in the semi-ring stub. The tuning of the Fano profile is realized by changing the size of the semi-ring stub, and the sensitivity and figure of merit of this structure is 575 nm/RIU and 5 671. Moreover, multiple fano resonances are induced by setting a rectangular cavity in the waveguide, a figure of merit as high as 6 555, which offer flexibility in the design of the structure. The waveguide structure may find widespread applications in highly integrated optical circuits, special for nano bio-sensor.

Key words: Surface plasmon polaritons; Nano sensor; Finite-difference time-domain method; Fano resonances; Semi-ring stub; Fano resonance
OCIS Codes: 240.6680; 230.7370; 230.4555; 280.4788

0 Introduction

Surfaceplasmon Polaritons (SPPs) are charge density waves that are formed by the interaction between free electrons and incident photons in a metal surface and propagate along the metal-dielectric interface[1]. SPPs are regarded as the most promising way for the realization of highly integrated optical circuits, due to their capability to overcome the classical optical diffraction limit and manipulate light transmission performance in the nanoscale domain[2], which provides possibility to realize nanoscale optical

Foundation item: The National Natural Science Foundation of China (Nos. 61502538, 61501525), the Nature Science Foundation for Young Scientists of Hunan Province, China (No. 2015JJ3157) and the Graduate Scientific Research Foundation of Central South University (No. 2017zzts699)
First author: GUO Yuan (1993—), female, M.S. degree candidate, mainly focuses on optoelectronics. Email: 152212047@csu.edu.cn
Supervisor (Contact author): XU Xue-mei (1971—), female, professor, Ph.D. degree, mainly focuses on optical applications. Email: xuxuemei999@126.com
Received: June.21, 2017; **Accepted**: Oct.10, 2017

devices with extraordinary property and compact integration in future[3]. Hence, photonic devices based on SPPs have extensive applications in super-resolution imaging[4], non-linear optics[5], subwavelength optical integration[6], and biochemical sensors[7].

In recent, theFano resonances in nano-plasmonic structure aroused more attentions for the reason that SPPs can breakthough the diffraction limit of light[2]. Fano resonance usually takes place between a discrete state and a continuous state, possessing a typical sharp and asymmetric line profile[8]. The devices based on the Fano resonance originating from a waveguide structure may obtain various optimal properties such as high sensitivity, strong high-Q and great a Figure Of Merit (FOM). Due to these distinctive traits, it has been widely studied in numerous physics systems including sensors[9], switches[10], wavelength demultiplexing[11], rings[12], photonic crystal[13], planar oligomers[14] and Metal-Insulator-Metal (MIM) waveguides[15]. Because the MIM waveguide's unique features support an acceptable propagation length for SPPs and confine light at a deep subwavelength scale[16-17], the Fano resonances are broad researched by using the MIM waveguides. In order to well tailor the light transmission spectra, it is extremely significant to fabricate a precise tuning Fano resonance. Up to now, different types of plasmonic structures have been discussed theoretically and experimentally, such as plasmonic nanoclusters[18], asymmetric T-shape single slits[19], and an asymmetric stub pair in MIM waveguides[20]. These research findings can not only lead people to understand the Fano resonance more profoundly, but also provides a feasible solution for the implementation of high sensitivity sensor.

In this paper, a novel symmetricplasmonic structure which consists of an MIM waveguide and a semi-ring stub is proposed and investigated by using the Finite-Difference Time-Domain (FDTD) method. It is found that the Fano resonance is generated by the interference between a discrete state and a continuous state in the semi-ring stub. Furthermore, the Fano resonance asymmetrical profile and the wavelength at the dip rely on the geometric parameters of the semi-ring stub, and the nanostructure is expected to work as an excellent plasmonic sensor with a high sensitivity of about 575nm/RIU and an FOM of about 5671. In addition, multiple Fano resonances are achieved by placing a rectangular cavity above the semi-ring stub horizontally. This new Fano formation mechanism, based on the different states, can be used in enhanced bio-chemical sensors and highly integrated circuits.

1 Structure and simulation

The MIM waveguide structure is shown in Fig. 1, where the blue and white areas presents metal and dielectric, respectively. It is made up of a semi-ringstub in a MIM bus waveguide, and the semi-ring stub symmetrically locates at a MIM bus waveguide. The main structural parameters are the width (h) of the waveguide, the outer radius (R) and inner radius (r) of the semi-ring stub. The width of the waveguide fixed to be $h = 50$ nm throughout the full text. The two power monitors are used at the points P_{in} and P_{out} of the waveguide to detect the incident power and the transmitted power, respectively. The transmission of the proposed structures is calculated by[21] $T = P_{out}/P_{in}$, and the transmission characteristics are investigated numerically and theoretically by using the FDTD method. We perform the FDTD simulation with boundary conditions (PML), dimensional (2D), mesh steps ($dx = dy = 5$ nm) and time step ($dt = dx/2c$, c is the velocity of light in vacuum).

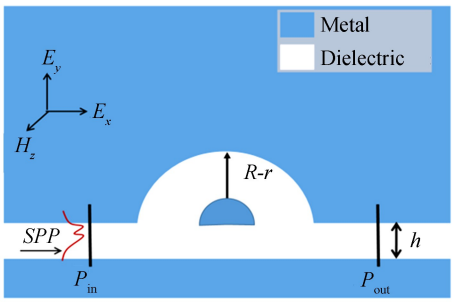

Fig.1 Scheme diagram of the plasmonic nano-sensor-based MIM waveguides

The guided modes inside the MIM waveguides are significantly affected by the effective refractive index n_{eff}, which can be obtained from the dispersion equation[22]

$$\varepsilon_m \sqrt{n_{eff}^2 - \varepsilon_d} \tanh\left(\frac{h\pi\sqrt{n_{eff}^2 - \varepsilon_d}}{\lambda}\right) + \varepsilon_d \sqrt{n_{eff}^2 - \varepsilon_m} = 0 \quad (1)$$

where h is the width of the waveguide, ε_m and ε_d are the dielectric constants of metal and dielectric,

respectively. ε_m is approximately described by the Drude model, which is defined as[23] $\varepsilon_m=\varepsilon_\infty-\omega_p^2/(\omega^2+i\omega\gamma)$, where ε_∞ is the dielectric constant at the infinite frequency, ω_p is bulk plasma frequency, ω is the angular frequency of incident light, and γ is the electron collision frequency. The parameters are $\varepsilon_\infty=3.7$, $\omega_p=9.1$ eV, $\gamma=0.018$ eV. Based on the Coupled Mode Theory (CMT), Φ is defined as the phase difference between the reflected SPPs and the transmitted SPPs, which is described as[24] $\Delta\Phi=4\pi n_{eff}l_{eff}/\lambda_m+\varphi$, where φ is the phase shift caused by the reflection of SPPs on the metal-dielectric interface, λ_m is the resonance wavelength, and l_{eff} is the effective length of SPPs in plasmonic structure. l_{eff} can be obtained by the following expression:

$$l_{eff}=\pi(R+r)/2 \tag{2}$$

When resonance condition is satisfied $\Delta\Phi=2m\cdot\pi$ (m is a positive integer and corresponds to the order of resonance mode). The wavelength of the Fano resonance dip will be determined by the length of the slot cavities. It can be expressed as[24]:

$$\lambda_m=4n_{eff}l_{eff}/(2m-\varphi/\pi) \tag{3}$$

Moreover, FOM as a key factor is widely used to evaluate the performance of theFano resonance. The Fano resonance detects rather a relative intensity change $dI(\lambda)/dn(\lambda)$ at fixed wavelength λ_0, and then FOM is defined as[25]

$$\mathrm{FOM}=\max\left|\frac{dI(\lambda)/dn(\lambda)}{I(\lambda)}\right| \tag{4}$$

$dI(\lambda)/dn(\lambda)$ is the relative intensity change at fixed wavelength induced by a refractive index change dn. $I(\lambda_0)$ corresponds to the intensity where FOM reaches a maximum value.

2 Results and discussions

Fig. 2 shows the transmission characteristics of the proposed structures. The blue curve in Fig. 2(a) represents the transmission spectrum of the semi-circle structure with $R=150$ nm, $r=0$ nm, and the semi-ring structure with $R=150$ nm, $r=50$ nm, respectively. It is obviously observed that a sharp and asymmetric profile emerges in the transmission spectrum. This sharp and asymmetric profile usually terms as Fano resonance profile[26]. Besides, the Fano resonance dip at 579 nm and peak at 635 nm, the magnetic

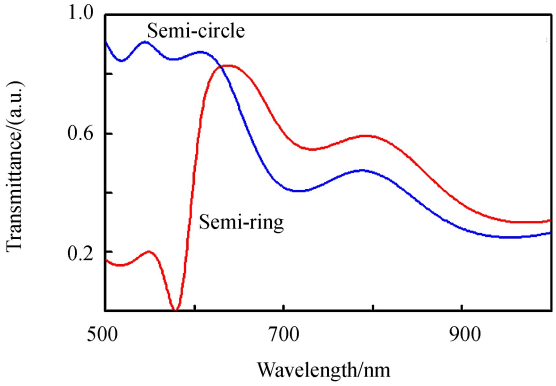

(a) Transmission spectra with different structure

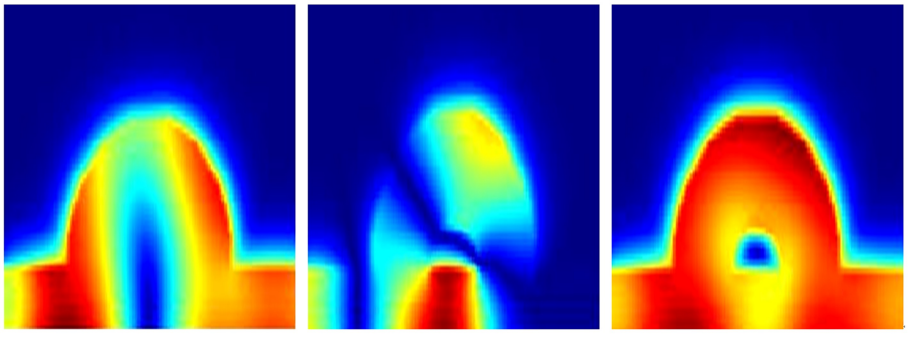

(b) λ=579 nm, r=0 nm (c) λ=579 nm, r=50 nm (d) λ=635 nm , r=50 nm

Fig.2 Transmission spectra and magnetic field distributions with different structure

field distributions of the semi-circle structure at 579 nm is shown in Fig. 2(b). Figs. 2(c)～(d) show the magnetic field distributions of the Fano resonance dip at 579 nm and peak at 635 nm. When the inner radius of the semi-ring stub $r=0$ nm, as a semi-circle structure, most of the SPPs is transported out. When the inner radius of the semi-ring stub $r=50$ nm, as a semi-circle structure, almost all of the SPPs is confined in the semi-ring stub, and no SPPs is transported out. When an incident light injects along the x-axis in the waveguide, a SPPs with the transverse-magnetic mode can be excited on the metal-dielectric interface and confined in the waveguide. One part of the SPPs propagate along the x-axis and pass through the waveguide, and the other part of the SPPs reflect back and forth in the semi-ring stub. Therefore, the Fano resonance will be generated because of the interference between a discrete state and a continuous state in the semi-ring stub. As can be seen from Figs. 2(c)～(d), at 579 nm, SPPs are almost blocked at the semi-ring stub, acted as the "off" state. While at 635 nm, SPPs can pass through the waveguide to the output port, served as the "on" state. In the all optical communication system, Fano profile is generally used to realize all-optical plasmonic switches[27], and the proposed structure achieved a sharp and asymmetric Fano profile, which has a wide application in the nano-sensing area.

We first investigate the transmission characteristics of thesemi-ring structure with different outer radius (R) when $r=50$ nm. By defining R as 130, 140, 150 and 160 nm, we obtain the transmission spectra in Fig. 3. The asymmetrical profile of the transmission spectrum presents an obvious transformation by increasing R. Specifically, the right side of the resonant valley maintains a high transmittance and increases rapidly with the increases of R. However, the Fano resonance dip without obvious movement. This phenomenon can be explained by Eq. (1) and (2), the effective refractive index (n_{eff}) decreases

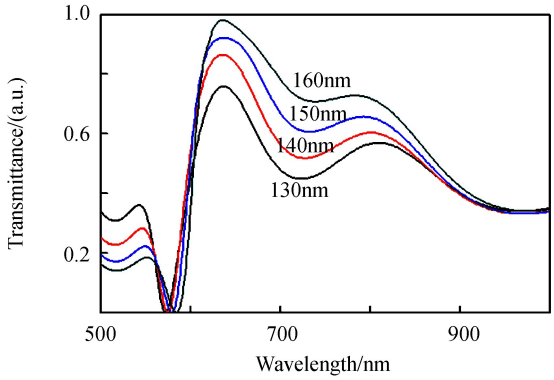

Fig.3 Transmission spectra of the semi-ring structure with different R when $r=50$ nm

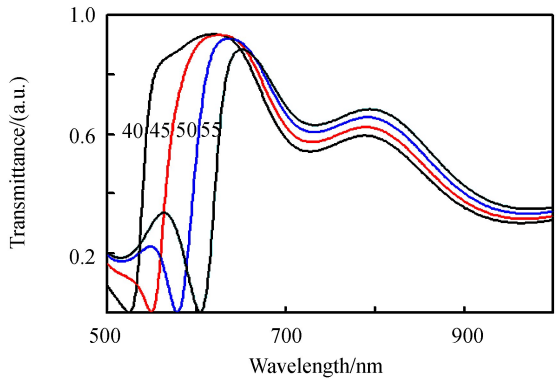

(a) Transmission spectra for different r

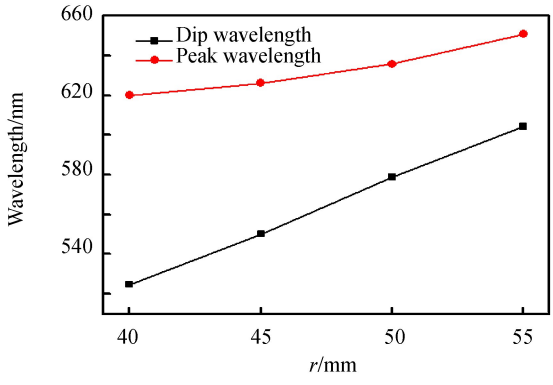

(b) Relations between r and resonance wavelength

Fig.4 Relation between r and the wavelength when $R=150$ nm

due to the width of the semi-ring stub increases as R increases, and the effective length (l_{eff}) increases as R increases. Therefore, according to Eq. (3), the resonance wavelengths (λ_{m}) increases are not very significant. Meanwhile, we explore the transmission characteristics of the semi-ring stub with different inner radius (r) when $R=150$ nm. The transmission spectra with various r are depicted in Fig. 4(a). The Fano resonance dip wavelengths are 524.7, 550.2, 578.9, and 604.1 nm when the inner radius of the semi-ring stub are 40, 45, 50, or 55 nm, respectively. It is worthwhile that the Fano resonance dip causes a redshift as r increases. This phenomena can be explained that the resonance wavelength (λ_{m}) grows by the rising of the effective refractive index (n_{eff}) and the increase of the effective length (l_{eff}) with increase of r, in accordance with Eq. (1), (2) and (3). Fig. 4(b) gives an analysis on the wavelength variations with respect to the inner radius of the semi-ring stub, with the increase of r from 40 to 55 nm with a step of 5 nm. It is found that the difference between the resonant peaks and dips decreases with the inner radius r

increasing, which may attribute to the internal loss decreases when the wavelength increases. According to the simulation results, the Fano resonance wavelengths can be easily manipulated by adjusting the inner radius of the semi-ring stub.

Lastly, we research the influence of the material embedded in the semi-ring structure on the Fano resonance wavelength. The resonant wavelength has a redshift when increasing the refractive index filled in the cavity. Figure 5(a) depicts the transmission spectra for different refractive indexes (n) when R = 150 nm and r = 50 nm, which indicates that the dip wavelengths and the peak wavelengths are at 578.9 and 635.7 nm, or 607.1 and 668.1 nm, or 635.7 and 699.9 nm, or 664.4 and 732.7 nm, or 693.1 and 764.2 nm when n = 1.00, 1.05, 1.10, 1.15, and 1.20, respectively. As can be seen from Fig. 5(b), it is found that both the transmitted peak and dip wavelength have a nearly linear relationship with the refractive index. As a result, one can simply manipulate the Fano resonance wavelength by fitting the material with appropriate refractive index in the semi-ring structure. The sensitivity (nm/RIU) is defined as the shift in the resonant wavelength per unit change of refractive index[25], as: $\Delta\lambda/\Delta n$, and the sensitivity of the proposed plasmonic nanosensor is about 575 nm/RIU. To better evaluate the performance of the plasmonic nanosensor, the FOM is further studied. Based on Eq. (4), the FOM of our designed plasmonic nanosensor is about 5671 by changing the refractive index from 1.00 to 1.20.

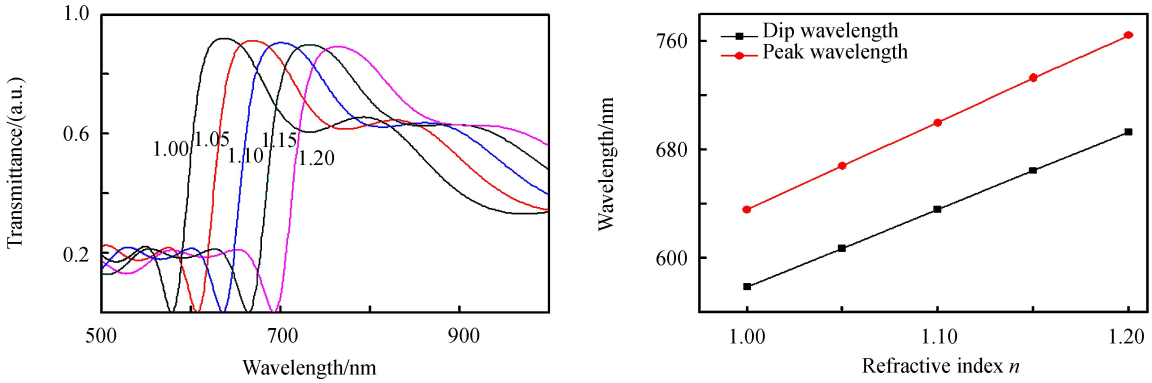

(a) Transmission spectra for different n (b) Relations between n and resonance wavelength

Fig.5 Relation between n and the wavelength when R = 150 nm, r = 50 nm

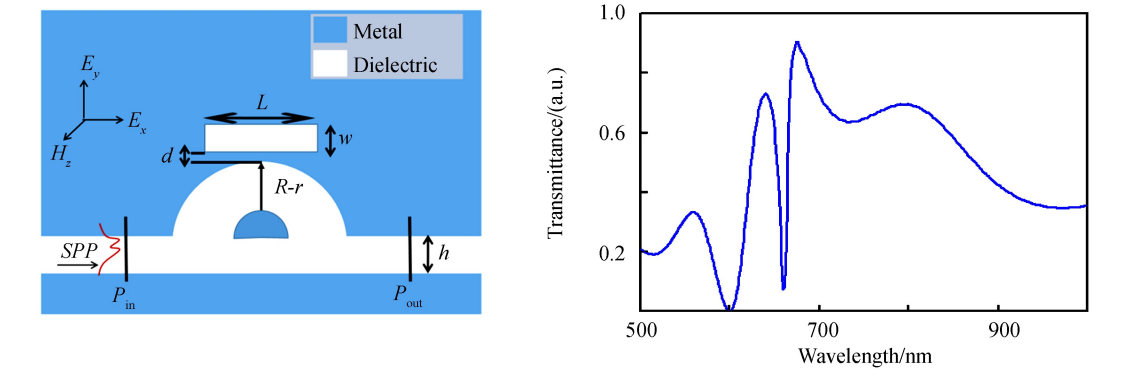

(a) Schematic diagram of multiple Fano resonances structure (b) Transmission spectrum of multiple Fano resonance structure

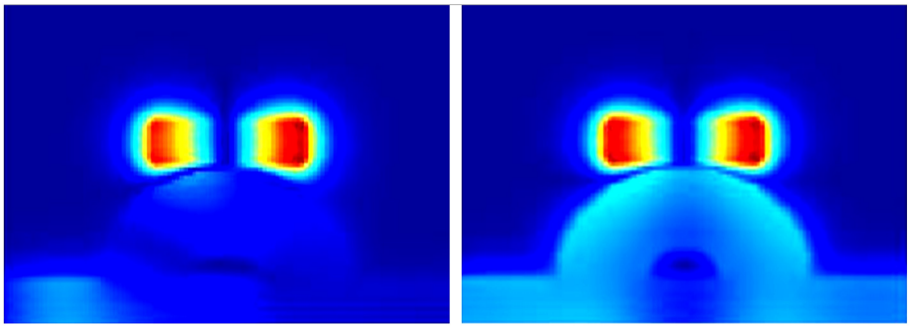

(c) λ= 660 nm, r=50 nm (d) λ=675 nm ,r=50 nm

Fig.6 Schematic diagram, transmission spectrum and magnetic field distributions of the multiple Fano resonance structure

Furthermore, one interesting phenomenon is also found and studied. As shown in Fig. 6(a), the proposed Fano structure in Fig. 1 can be extended to a multiple Fano resonances structure by setting a rectangular cavity in the waveguide, which is horizontally placed above on the semi-ring stub. By defining the length $L=180$ nm and width $w=50$ nm of the rectangular cavity, and the coupling distance $d=10$ nm from the rectangular cavity to the semi-ring stub with $h=50$ nm, $R=150$ nm and $r=50$ nm, we can also obtain the transmission spectrum in Fig.6 (b). The first Fano resonance dip presents at about 600 nm, which is called FR 1 in the following article. The second Fano resonance dip presents at about 660 nm and is called FR 2 in the following article. Figs. 6(c)～(d) shows the magnetic field distributions of the second Fano resonance dip at 660 nm and peak at 675 nm. Obviously, after light transmitting into the semi-ring stub, SPPs will be coupled into the rectangular cavity with narrowband spectral responses. Since the semi-ring stub structure provides broad pass band, the second Fano resonance will then be generated because of the interaction of two modes.

The influence of the structure parameters on the transmission spectrum is studied in detail and the results are shown in Fig.7. Figure 7(a) depicts that the position of FR1 can be tuned by the inner radius (r) of the semi-ring stub. As shown in Fig. 7(a), with r increasing from 45 nm to 60 nm, the position of the FR 1 changes from about 547 nm to about 627 nm, and simultaneously, almost no change in the position of FR 2 (<2 nm). Figure 7(b) depicts that the position of the FR 2 can be tailored by the length of the rectangular cavity L. As shown in Fig. 7(b), with increasing L from 180 nm to 210 nm, the position of the FR 2 changes from 660 nm to 737 nm. At the same time, the change in FR 2 position is small, only about 2 nm. Due to the independent tenability of the narrow states of FR 1 and FR 2, the two Fano resonances can be tuned independently. When the parameters of the structure are $L=180$ nm, $w=50$ nm, $d=10$ nm, $h=50$ nm, $R=150$ nm and $r=50$nm, as shown in Fig. 8, with the increasing of n from 1.00 to 1.20, the dips of FR 1 and FR 2 are both redshift. The dips of FR 1 red shifts from about 600 nm to 718 nm and the dips of FR 2 red shifts from about 660 nm to 790 nm. Our results deeply explore the dispersion principle of MIM waveguide. Furthermore, FOM is provided to investigate the performance of the sensor by changing the refractive index from 1.00 to 1.20. There are two dips with FOM of 6555 and 145 at the wavelengths of 600 and 660 nm, respectively.

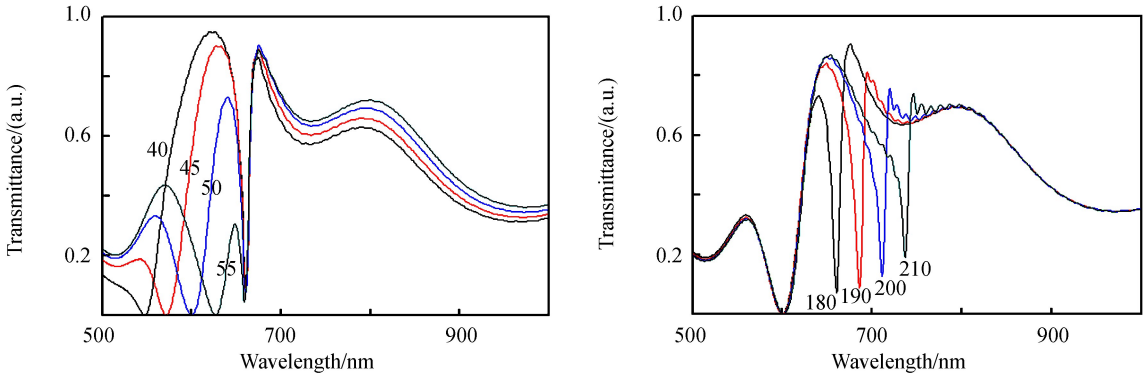

(a) Different r with fixed L=180 nm (b) Different L with fixed r=50 nm

Fig.7 Transmission spectra of the multiple Fano resonance structure when $R=150$ nm, $w=50$nm, $d=10$nm

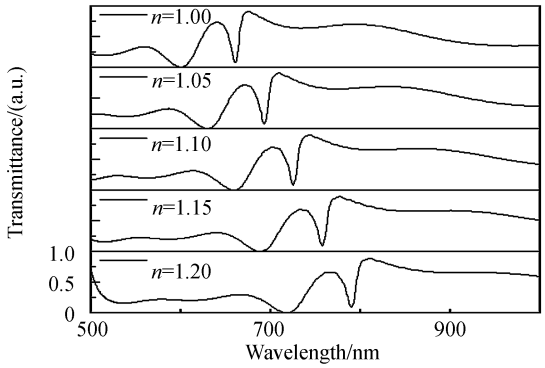

Fig.8 Transmission spectra of the multiple Fano resonances structure with different n when $R=150$ nm, $r=50$ nm, $L=180$ nm, $w=50$ nm, $d=10$ nm

3 Conclusion

In summary, the transmission characteristics of the proposed structure, which consists of a MIM waveguide with a semi-ring stub, are analyzed and investigated. Simulation results show that a sharp transmission dip was achieved at a broad wavelength range. The asymmetrical line shape and the resonance wavelength can be manipulated by changing the outer radius and inner radius of the semi-ring stub, respectively. The sensitivity and the FOM were 575 nm/RIU and 5 671. In addition, multiple Fano resonances are attached by placing a rectangular cavity above the semi-ring stub horizontally. In this case, the two Fano resonances can be tuned independently through changing the length of the rectangular cavity and the inner radius of the semi-ring stub, respectively. In our designed structure, the highest FOM reached to 6 555. Some challenges that we may be faced if the device was actually made to the practical applications. We will do our best to realize such a thin free-standing structure at a thickness of 10 nm, and to avoid the infiltrated fluids damaging the thin Ag spacers in the context of the current technology. Anyhow, the proposed structure achieved a sharp and asymmetric Fano profile, which has a wide application in the plasmonic nano-sensing area.

References

[1] BARNES W L, DEREUX A, EBBESEN T W. Surfaceplasmon subwavelength optics[J]. *Nature*, 2003, **424**(6950): 824-830.

[2] PARK J, KIM K Y, LEE I M, *et al*. Trapping light in plasmonic waveguides[J]. *Optics express*, 2010, **18**(2): 598-623.

[3] GAN Qiao-qiang, GAO Yong-kang, WANG Qing, *et al*. Surface plasmon waves generated by nanogrooves through spectral interference[J]. *Physical Review B*, 2010, **81**(8): 085443.

[4] ZHU Peng, SHI Hao-fei, Guo L J. SPPs coupling induced interference in metal/dielectric multilayer waveguides and its application for plasmonic lithography[J]. *Optics Express*, 2012, **20**(11): 12521-12529.

[5] RENGER J, QUIDANT R, VAN H N, *et al*. Free-space excitation of propagating surface plasmon polaritons by nonlinear four-wave mixing[J]. *Physical Review Letters*, 2009, **103**(26): 266802.

[6] SORGER V J, OULTON R F, MA R M, *et al*. Toward integrated plasmonic circuits[J]. *MRS Bulletin*, 2012, **37**(8): 728-738.

[7] BROLO A G.Plasmonics for future biosensors[J]. *Nature Photonics*, 2012, **6**(11): 709-713.

[8] LUKYANCHUK B, ZHELUDEV N I, MAIER S A, *et al*. The Fano resonance in plasmonic nanostructures and metamaterials[J]. *Nature Materials*, 2010, **9**(9): 707-715.

[9] LU Hua, LIU Xue-ming, MAO Dong, *et al*. Plasmonic nanosensor based on Fano resonance in waveguide-coupled resonators[J]. *Optics letters*, 2012, **37**(18): 3780-3782.

[10] HEUCK M, KRISTENSEN P T, ELESIN Y, *et al*. Improved switching using Fano resonances in photonic crystal structures[J]. *Optics Letters*, 2013, **38**(14): 2466-2468.

[11] CHEN Zhao, HU Ru, CUI Luna, *et al*. Plasmonic wavelength demultiplexers based on tunable Fano resonance in coupled-resonator systems[J]. *Optics Communications*, 2014, **320**(2): 6-11.

[12] FU Yuan-hsing, ZHANG Jing-bo, YU Ye-feng, *et al*. Generating and manipulating higher order Fano resonances in dual-disk ring plasmonic nanostructures[J]. *ACS Nano*, 2012, **6**(6): 5130-5137.

[13] NOZAKI K, SHINYA A, MATSUO S, *et al*. Ultralow-energy and high-contrast all-optical switch involving Fano resonance based on coupled photonic crystal nanocavities[J]. *Optics Express*, 2013, **21**(10): 11877-11888.

[14] BROWN L V, SOBHANI H, LASSITER J B, *et al*. Heterodimers: plasmonic properties of mismatched nanoparticle pairs[J]. *ACS Nano*, 2010, **4**(2): 819-832.

[15] WANG Jun-qiao, FAN Chun-zhen, HE Jin-na, *et al*. Double Fano resonances due to interplay of electric and magnetic plasmon modes in planar plasmonic structure with high sensing sensitivity[J]. *Optics Express*, 2013, **21**(2): 2236-2244.

[16] JIANG Ya-lan, WANG Ji-cheng, WANG Yue-ke, *et al*. A MIM surface plamson T-splitter based on a stub structure [J]. *Acta Photonica Sinica*, 2014, **43**(9): 0923002.

[17] ZHENG Ming-fei, LI Hong-jian, XU Hui, *et al*. Filtering property based on ultra-wide stopband in double sector/sectorial-ring stub resonator coupled to plasmonic waveguide[J]. *IEEE Photonics Journal*, 2017, **9**(5): 2201308.

[18] LASSITER J B, SOBHANI H, FAN J A, *et al*. Fano resonances in plasmonic nanoclusters: geometrical and chemical tunability[J]. *Nano Letters*, 2010, **10**(8): 3184-3189.

[19] CHEN Jian-jun, LI Zhi, YUE Song, *et al*. Plasmon-induced transparency in asymmetric T-shape single slit[J]. *Nano Letters*, 2012, **12**(5): 2494-2498.

[20] PIAO Xian-ji, YU S, PARK N. Control of Fano asymmetry in plasmon induced transparency and its application to

plasmonic waveguide modulator[J]. *Optics Express*, 2012, **20**(17): 18994-18999.

[21] CAO Guang-tao, LI Hong-jian, YANG Hui, *et al*. Uniform theoretical description of plasmon-induced transparency in plasmonic stub waveguide[J]. *Optics Letters*, 2014, **39**(2): 216-219.

[22] LU Hua, LIU Xue-ming, MAO Dong. Plasmonic analog of electromagnetically induced transparency in multi-nanoresonator-coupled waveguide systems[J]. *Physical Review A*, 2012, **85**(5): 053803.

[23] QI Ji-wei, CHEN Zong-qiang, CHEN Jing, *et al*. Independently tunable double Fano resonances in asymmetric MIM waveguide structure[J]. *Optics Express*, 2014, **22**(12): 14688-14695.

[24] ZHENG Ming-fei, LI Hong-jian, CHEN Zhi-quan, *et al*. Compact and multiple plasmonic nanofilter based on ultra-broad stopband in partitioned semicircle or semiring stub waveguide[J]. *Optics Communications*, 2017, **402**: 47-51.

[25] BECKER J, TRUGLER A, JAKAB A, *et al*. The optimal aspect ratio of gold nanorods for plasmonic bio-sensing[J]. *Plasmonics*, 2010, **5**(2): 161-167.

[26] FANO U. Effects of configuration interaction on intensities and phase shifts[J]. *Physical Review*, 1961, **124**(6): 1866.

[27] CHEN Jian-jun, LI Zhi, ZHANG Xiang, *et al*. Submicron bidirectional all-optical plasmonic switches[J]. *Scientific Reports*, 2013, **3**(3): 1451.